Received: 9 June 2022 | Revised: 15 July 2022 | Accepted: 22 July 2022

DOI: 10.1002/pat.5817

RESEARCH ARTICLE

polymers for advanced technologies WILEY

Porous chitosan particles doped by in situ formed silver nanoparticles: Electrorheological response in silicon oil

Nikita M. Kuznetsov[1] | **Victoria V. Kovaleva**[1] | **Danila A. Volkov**[1] | **Yuriy D. Zagoskin**[1] | **Artem Yu. Vdovichenko**[1,2] | **Sergey N. Malakhov**[1] | **Artem V. Bakirov**[1,2] | **Eugeny V. Yastremsky**[1,3] | **Roman A. Kamyshinsky**[1,3,4] | **Alexei A. Stupnikov**[1] | **Sergei N. Chvalun**[1,2] | **Timofei E. Grigoriev**[1,4]

[1]Laboratory of Polymer Materials, Nanobiomaterials and Structures Department, National Research Center "Kurchatov Institute", Moscow, Russia

[2]Laboratory of Functional Polymer Structures, Department of Biopolymers, Enikolopov Institute of Synthetic Polymeric Materials of Russian Academy of Sciences, Moscow, Russia

[3]Laboratory of Electron Microscopy, Shubnikov Institute of Crystallography, Federal Research Center "Crystallography and Photonics", Russian Academy of Sciences, Moscow, Russia

[4]Institute of Nano-, Bio-, Information, Cognitive and Socio-humanistic Sciences and Technologies, Moscow Institute of Physics and Technology, Dolgoprudny, Moscow Region, Russia

Correspondence

Nikita M. Kuznetsov, Laboratory of Polymer Materials, Nanobiomaterials and Structures Department, National Research Center "Kurchatov Institute", 1, Akademika Kurchatova pl., Moscow, 123182, Russia.
Email: kyz993@yandex.ru

Funding information

Ministry of Science and Higher Education of the Russian Federation; Russian Science Foundation

Abstract

Effect of in situ formed silver nanoparticles doping on electrorheological response of highly porous chitosan particles in suspensions of polydimethylsiloxane (silicone oil) is considered. Silver nanoparticles are directly reduced by chitosan from solution. Highly porous chitosan particles with different silver content are fabricated by spraying from solution followed by freeze-drying. A high and stable electrorheological response of suspensions in wide range of electric field strength is observed at a very low filler content of 1 wt%. The nature of the electrorheological effect is considered from the standpoint of dielectric spectroscopy. The activation energies of polarization processes are determined from the temperature dependences of the dielectric loss modulus. The study shows the opportunity to control the properties of stimuli-responsive materials by changing the structure and physicochemical properties of the functional filler. This approach opens up new possibilities for creating materials with high performance and predetermined properties.

KEYWORDS

chitosan, colloids, electrorheological fluids, silver nanoparticles, stimuli-responsive materials

1 | INTRODUCTION

Wide possibilities for applications Chitosan is a polysaccharide, a derivative of chitin, the second most abundant polymer in nature. This polymer has a large number of free amino and hydroxyl side groups, which results in combination of various unique physicochemical properties.[1] Chitosan is a biodegradable, biocompatible and non-toxic polymer,[2,3] with pronounced antimicrobial and antioxidant properties.[4,5] The listed properties make chitosan materials attractive for researchers due to the great application possibilities in regenerative medicine,[6,7] flexible compact wearable devices such as energy storage devices, biosensors, probes, etc.[8,9]

One of the shortcomings of chitosan matrices for electronic devices is insufficient electrophysical characteristics such as dielectric permittivity and conductivity. Therefore, to improve these parameters, chitosan is doped with weak acids,[10] conductive polymers,[11] or inorganic nanostructured additives,[12,13] various metal ions and nanoparticles (Fe, Cu, Ag, Au etc.).[14–16] Silver nanoparticles have several advantages over other dopants, while highly conductive ($\sim 6 \times 10^7$ S cm^{-1}), silver is less likely to oxidize or corrode. Due to its original characteristics, silver is used for antibacterial materials,[17–19] as well as additives to improve the physical properties of materials.[20] For instance, polymer composites pastes with silver nanoparticles have excellent electrical and thermal conductivity, which is applicable to LED packages and various electronic applications.[21,22] In addition, silver nanoparticles are actively considered for sensors because of their superior optical properties.[23,24] Combined with polymers, silver is useful for flexible conductive materials for wearable electronics.[25,26]

It should be noted that silver nanoparticles could be reduced in solution by chitosan from silver nitrate. Thus, chitosan acts as a reductant and prevents the strong aggregation of nanoparticles during synthesis.[27,28] It is possible to achieve a chitosan-silver composite with the most optimal properties for specific applications by varying some parameters, such as the concentration of chitosan and silver, the molecular weight of chitosan, temperature, recovery time, etc.

One of the modern applications of chitosan is as a filler for electrorheological fluids (ERFs). ERFs are smart materials capable of fast and reversible transition from viscous to solid state under external electric field. Typically, ERFs are suspensions consisting of liquid dielectric media, often silicone oil, and easily polarizable filler particles.[29] The main mechanism of the effect is associated with differences in the dielectric permittivity and conductivity of the filler and the medium leading to polarization of particles in electric field and columnar structures formation.[30] ERFs have great potential in various fields of technology such as dampers, clutches, robotics, sensors, microfluidics etc.[31] That is why the search for new fillers revealing electrorheological activity is an urgent task.

Suspensions of chitosan in dielectric liquids are ERFs. Degree of deacetylation affects the electrophysical properties of chitosan and as a result the intensity of the electrorheological effect. Thus, pristine chitin and chitosan with a very high degree of deacetylation show reduced efficiency compared to average degrees of deacetylation, when a balance between amino and aceto groups is achieved, resulting in enhanced value of dielectric permittivity.[32] However, it is known that a high electrorheological response can be achieved through the additional particle shape effect.[33,34] Particles with a high aspect ratio are oriented under an electric field and are able to form a percolation network at fillings of just several wt%. The pronounced orientation of anisometric particles leads to an increase in the electrorheological effect in contrast with isotropic fillers.[35–39] Recently, a high electrorheological response of chitin nanorods with an aspect ratio of ~70 was reported. The fluid reveals stable response with electric field strengths up to 7 kV mm^{-1}, and the yield stress reaches about 220 Pa at the filler concentration of 1 wt%.[40]

Utilizing fillers with porous structure opens up new perspectives for the development of ERFs.[41,42] Recently, highly porous chitosan particles were considered as filler for ERFs.[43] Preliminary formation of a polymer mesh combined with interpenetrating macropores in the particle structure results in extremely high sedimentation stability and electrorheological response even at 1 wt% of filler content. The yield stress of such fluid reaches ~600 Pa at 7 kV mm^{-1}. Similar performance is typically shown by fluids with an order of magnitude higher filler content.[44–46] Moreover, such fluids show stable response in a wide temperature range which is of great importance for real practical application.[47] The natural oils and fillers allow to create completely eco-friendly ERFs,[48–50] so polysaccharides are promising candidates from this point of view as well.[51,52]

One of the ways to increase the electrorheological response is to change the electrophysical characteristics of the filler with surface modification or doping.[53–55] Several studies have shown that the incorporation of small inclusions into the structure of the filler leads to a change in the polarizability of the particles and optimization of the relaxation time, which significantly enhance the electrorheological response of fluids. For example, TiO_2 particles inlaid with nanocarbon clusters with jujube cake structure[56] and TiO_2-based ionogel nanoparticles (TiO_2-[D_{sim}]Cl) were obtained as fillers. Thus, the combination of two approaches, such as the formation of a developed highly porous structure of the filler and the incorporation of electrosensitive nanoparticles into it, will allow the development of novel effective ERFs. The fundamental possibility of a composite highly porous chitosan particles production was shown previously by cellulose doping.[57] The aim of this study was to verify if the silver nitrate content in chitosan solution affects the kinetics of silver nanoparticles reduction and adjusts the electrorheological behavior of porous chitosan/silver particles in silicon oil.

2 | MATERIALS AND METHODS

2.1 | Preparation of filler particles

Chitosan (ChitoClear 43000—HQG 10, Primex, Iceland) with an average molecular weight of 80 kDa[58] and silver nitrate ($AgNO_3$, ACS Reagent, ≥99.0%, Honeywell Fluka, USA) were used for the preparation of precursor solutions. The chitosan/silver nitrate solutions of 1 wt% in a 2 wt% aqueous acetic acid with a ratio of components by weight 1/0.10, 1/0.21, 1/0.52 and 1/1.04 were obtained and kept in a dark place at a temperature of 60 °C for 5 days for the growth of silver nanoparticles. From here on the filler composition is denoted according to these component ratios. The maturation time was optimized according to spectrophotometry and cryo-electron microscopy studies. Filler particles were obtained according to the universal method proposed previously.[59] Briefly, the selected dispersion was sprayed into a bath of liquid nitrogen to form frozen spherical particles. Next, the particles were collected and kept at a temperature of −24°C to remove nitrogen, followed by freeze-drying via Alpha 2–4 LDplus (Martin Christ, Germany) for 3 days at 0.250 mbar with following final drying at 0.030 mbar within 10 h until the frozen solvent (acetic acid solution) was completely removed. Low concentration of pristine solutions provides high porosity of the received particles.

2.2 | Preparation of ERFs

ERFs were prepared as follows. The required amount of porous composite particles of selected composition were dispersed into the silicon oil (low molecular weight polydimethylsiloxane – PDMS) (PMS-100, Penta Junior LLC, Russia) by a magnetic stirrer during 48 h until a homogeneous suspension was formed. The average PMS-100 molecular weight (M_w) of 12.0 kDa and polydispersity index of 2.0 were determined by size exclusion chromatography using RI detector Smartline RI 2400 (Knauer, Germany). The concentration of ERFs with fillers of various composition was 1 wt%. The filler volume fraction depends on the ratio of chitosan to silver and is estimated in Table S1. Before measurements all samples were sonicated for 20 min by UZV-4.0/1 TTTs (RMD) ultrasonic bath (150 W, 35 kHz) (Sapfir LLC, Russia). The colloidal stability of suspensions was evaluated by sedimentation ratio of colloid phase height to total fluid height during 90 days due to high viscosity of dispersion media and slow sedimentation process.

2.3 | Ultraviolet–visible spectrophotometry

The formation of silver nanoparticles was controlled by Ultraviolet–visible (UV) spectrophotometry using UV-3000 (Shimadzu, Japan) instrument in transmission mode in the wavelength range of 300–800 nm. Dispersions of 1 wt% chitosan in 2 wt% acetic acid with different content of $AgNO_3$ (ratios 1/0.10, 1/0.21, 1/0.52 and 1/1.04) were measured in quartz cuvettes (Hellma 100-QS), the optical path length was 10 mm. Since the effective optical density of the samples exceeded 4 abs., the optical path length was reduced down to 2 mm. The data were normalized to the corresponding difference in optical path length in the final spectrophotometric data plots. Since the effective optical density at a path length of 2 mm exceeded 4 abs. again, the samples were diluted with 2 wt% acetic acid solution, followed by normalization of the results by the degree of dilution. Thus, UV spectrophotometric data were obtained for dispersions over a period up to 60 days with measured effective absorbance up to 60 abs.

2.4 | Cryo-transmission electron microscopy

Lacey carbon grids (Ted Pella, USA) were glow-discharged with PELCO easiGlow (Ted Pella, USA) at 25 mA plasma current for 30 s and 3 μl aliquots of sample solutions were applied onto them afterward. Then samples were rapidly plunge-frozen in liquid ethane using Vitrobot Mark IV (Thermo Fisher Scientific, USA) after blotting for 1.5 s using filter paper at 4°C and 100% humidity. Resulting vitrified samples were examined with Titan Krios (Thermo Fisher Scientific, USA) cryo-TEM equipped with spherical aberration image corrector (CEOS, Germany) at 300 kV in low dose mode using EPU software.

2.5 | Scanning electron microscopy

SEM imaging and EDX analysis were performed using a Phenom XL instrument (Thermo Fisher Scientific, USA) equipped with backscattered and secondary electron detectors, as well as Amptek X-123SDD EDX detector. Pressure was 0.1 Pa, an accelerating voltage was 5 kV for SEM imaging and 15 kV for EDX analysis.

2.6 | Fourier transform infrared spectroscopy

The composition of the composite fillers and pristine chitosan was studied by Fourier transform infrared spectroscopy (FTIR) with a Nicolet iS5 FTIR spectrometer (Thermo Fisher Scientific, USA) using an iD5 ATR accessory. The study was performed in the range of 550–4000 cm^{-1}.

2.7 | Optical microscopy

Frozen chitosan particles doped by silver nanoparticles were studied by polarized optical microscopy using Axio Imager.M2m microscope (Carl Zeiss, Germany) in the crossed polarized light condition. Temperature conditions of $-10\,^{\circ}C$ were achieved by means of cooling system LNP95 with a Linkam stage THMSG600. Particles from the dispersion in liquid nitrogen were applied to a glass slide using a pre-cooled spatula to avoid sample melting. Next, the glass slide was quickly placed in the Linkam stage under the measurement conditions. Images were obtained at various magnifying powers. Image analysis was performed using Axio Vision software. Series of microphotographs taken at various focus distances were joined resulting in a single focused image using the "Stack focusing" algorithm with ImageJ software.[60] Algorithm finds particle edges in each image inside the series and then joins them.

2.8 | X-ray scattering

The small (SAXS) and wide (WAXS) angle X-ray scattering studies were performed at BioMur beamline of Kurchatov synchrotron radiation source (Russia, Moscow). The wavelength was $\lambda = 1.445$ Å and the 2D detector was Dectris Pilatus 1 M. The distance between sample cell and detector was varied from 150 to 2500 mm. Filler powders were examined in open-ring cells. The exposure time depended on the scattering intensity of the sample and varied from 10 to 300 s for studies in small and wide angles, respectively. Silver behenate ($d_{001} = 58.38$ Å) was used as reference in all tests. Primary processing of 2D images was carried out using the Fit2D program. The primary processing of the SAXS data was performed using an open source software ATSAS.[61]

2.9 | Rotational viscometry

Rheological behavior of suspensions were studied on Physica MCR 501 rheometer (Anton Paar, Germany) equipped by two coaxial cylinders measuring cell (CC-27E) in the range of electric field strengths from 0 to 7 $kV\,mm^{-1}$. The electric field was supplied from the constant high voltage source FuG HCP 14–12500 MOD (FuG Elektronik GmbH, Germany). The flow and viscosity curves were detected in control shear rate (CSR) mode in the range of shear rate from 0.01 to 1000 s^{-1}. The dependence of the static yield stress on the electric field strength was measured in control shear stress (CSS) mode. To determine the loss and storage moduli the dynamic measurements in oscillation mode were performed at the strain amplitude value of 0.1% in the linear range of viscoelasticity. All data were obtained at the temperature of 20°C. The data were processed by the Rheoplus 3.40 software.

2.10 | Dielectric spectroscopy

The Novocontrol Alpha-A high-resolution impedance analyzer with the Quatro Cryosystem temperature control system and ZGS Alpha-A active sample cell equipped with Liquid Parallel Plate Sample Cell Novocontrol BDS1308 (Novocontrol Technologies GmbH & Co. KG, Germany) was used to collect impedance spectra in the temperature range from 0°C to 50°C in steps of 5°C. As-prepared ERFs under study were loaded into liquid sample cell. The distance between disk electrodes was separated by a Teflon spacer of 2 mm, the sample area was 214 mm^2. Measurements were performed at an excitation voltage of 1 V_{RMS}.

3 | RESULTS AND DISCUSSION

One of the goals of the study was to obtain highly porous chitosan microparticles with inclusions of silver nanoparticles homogeneously distributed in the polymer structure. Therefore, the aspect of growth and agglomeration of silver nanoparticles in the stock solution became fundamental. The process of nanoparticle formation was studied by UV-spectrophotometry and cryo-TEM. Already a day after the preparation of the dispersions, the corresponding UV-spectra show a specific maximum in the region of 420 nm corresponding to the surface plasmon resonance (SPR) on the silver nanoparticles (**Figure** 1A). The higher the nanoparticles content in the solution, the higher the intensity maximum. The position of the peak is determined by the chemical nature and size of the nanoparticles (silver in our study), and its width is associated with polydispersity. Obviously, the intensity of the maximum depends on the amount of formed nanoparticles, and it is higher the higher the ratio of silver to chitosan. In addition, we note that the broadening of the SPR peak is more pronounced at a low ratio, which is associated with the growth of nanoparticles. Thus, after reduction, silver atoms form clusters and then nanoparticles. In the case of an excess of the reducing agent content, that is, a low content of silver salt compared to chitosan, the diffusion path of reduced atoms and clusters of silver to the crystallization center is significantly greater than in the case of a high content of nitrate in solution. Therefore, at the early stages of reduction, the dispersion of nanoparticles exhibits a high polydispersity and a low absorbance. Over time, the intensity of the peak increases for all samples, and the polydispersity of the particles decreases (Figure 1B). The peak area was used to determine the relative optical density of the samples corresponding to the relative degree of silver reduction and nanoparticles formation. Then the corresponding kinetic curves were obtained (Figure 1C). It can be seen that, at the initial stage, the rate of silver nanoparticles formation is constant: the relative intensity of SPR increases linearly with time.

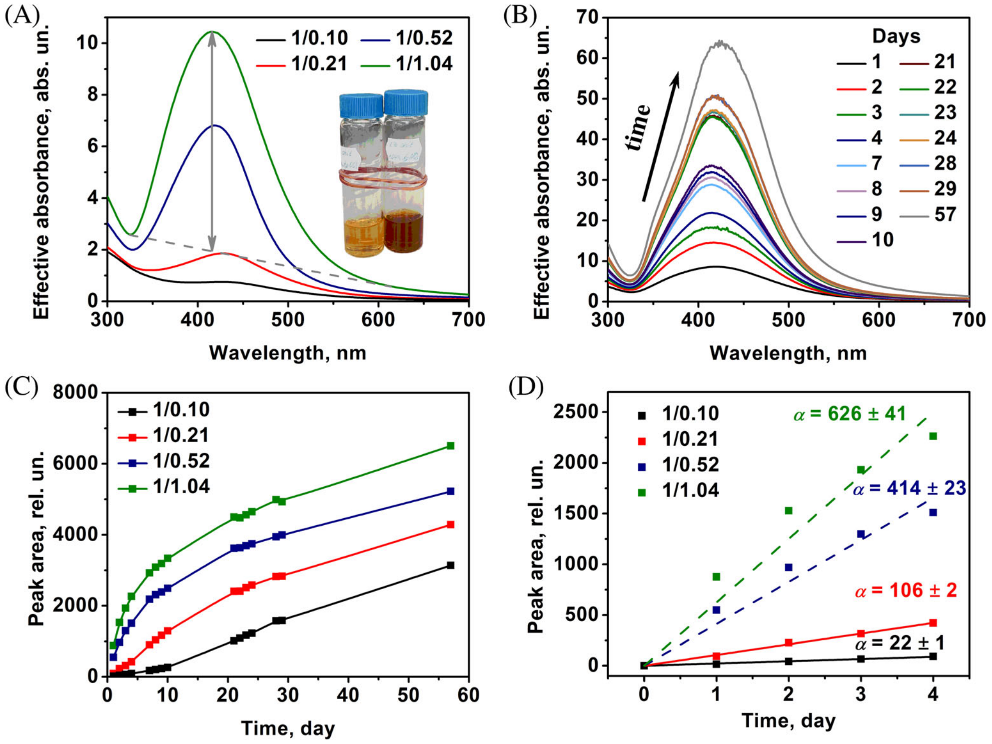

FIGURE 1 (A) UV spectra of chitosan/silver dispersions after heating at 60°C for one day. The inset shows typical dispersions at chitosan/silver ratio of 1/0.10 and 1/1.04. The concentration can be distinguished by the color saturation of the colloidal solution. (B) Evolution of UV spectra of dispersion at chitosan/silver ratio of 1/1.04 during several days after heating at 60°C. (C) Optical density peak area of dispersions with different chitosan/silver ratio over time. (D) Analysis of the silver nanoparticles reduction rate in solution during the first several days. The slope α corresponds to the relative reduction rate

Further, the dependence changes and the rate of the process slows down, which is expressed in a time dependence slope change. Note that the duration of the stage with linear dependence is affected by the ratio of chitosan to silver in the dispersions as well, and it is longer in the case of an excess of chitosan. This can be explained by the fact that, in addition to decreasing the $AgNO_3$ concentration in the solution, the kinetics of the process is also affected by the chitosan content acting as a reducing agent. Previously, it was shown that at a constant concentration of $AgNO_3$ and an increase in the concentration of chitosan, a greater amount of silver is reduced during 48 h.[28] This means that in our case, with an increase in the concentration of silver salt in the solution, the reduction potential of chitosan decreases, which leads to an earlier slowdown of the process. It is important that even after 60 days the process of silver reduction and nanoparticle growth continues. The mechanism of silver ions reduction from solution by chitosan molecules and further growth of particles is still not completely clear. Several reactions are expected to take place.[28] Probably, the process is multi-route, and can also be complicated by nanoparticles aggregation. Thus, it cannot be described by traditional kinetic equations. Figure 1D shows linear approximation of the initial stage of the effective absorbance evolution over time. It can be seen that deviation from linearity is observed at a close chitosan to silver ratio even in the first few days. At the same time, the slope of the dependences also differs for dispersions with the different ratio of components. That is, the higher the concentration of silver in the solution, the more intense the reduction process.

The uniformity of the dopant distribution (in our study of silver nanoparticles) in the polymer matrix is important when polymer composite filler is produced. Thus, the aggregation of nanoparticles should be avoided. The native structure of an acetic acid solution of chitosan at different periods of reduction was examined by the cryo-TEM method to study the processes of nanoparticles growth (Figure 2). The method makes it possible to avoid the artifact agglomeration during the sample preparation due to the procedure of rapid freezing of a thin layer leading to formation of amorphous ice. Note that the images show the formation of nanoparticles even on the first day after preparation of solutions, which correlates with UV spectroscopy data. While the concentration of nanoparticles was quite low for the solution excess of chitosan (Figure 2A), single nanoparticles and occasional agglomerates were still observed (inset in Figure 2A). A similar picture was observed with an increase in the concentration of silver in solution. For example, a sufficiently large number of polydisperse nanoparticles (Figure 2C) and occasional agglomerates (Figure 2C inset) were formed on the first day after solution preparation at the chitosan to silver ratio of 1/1.04. The appearance of accompanying particles of small sizes in the cryo-TEM images can be associated with

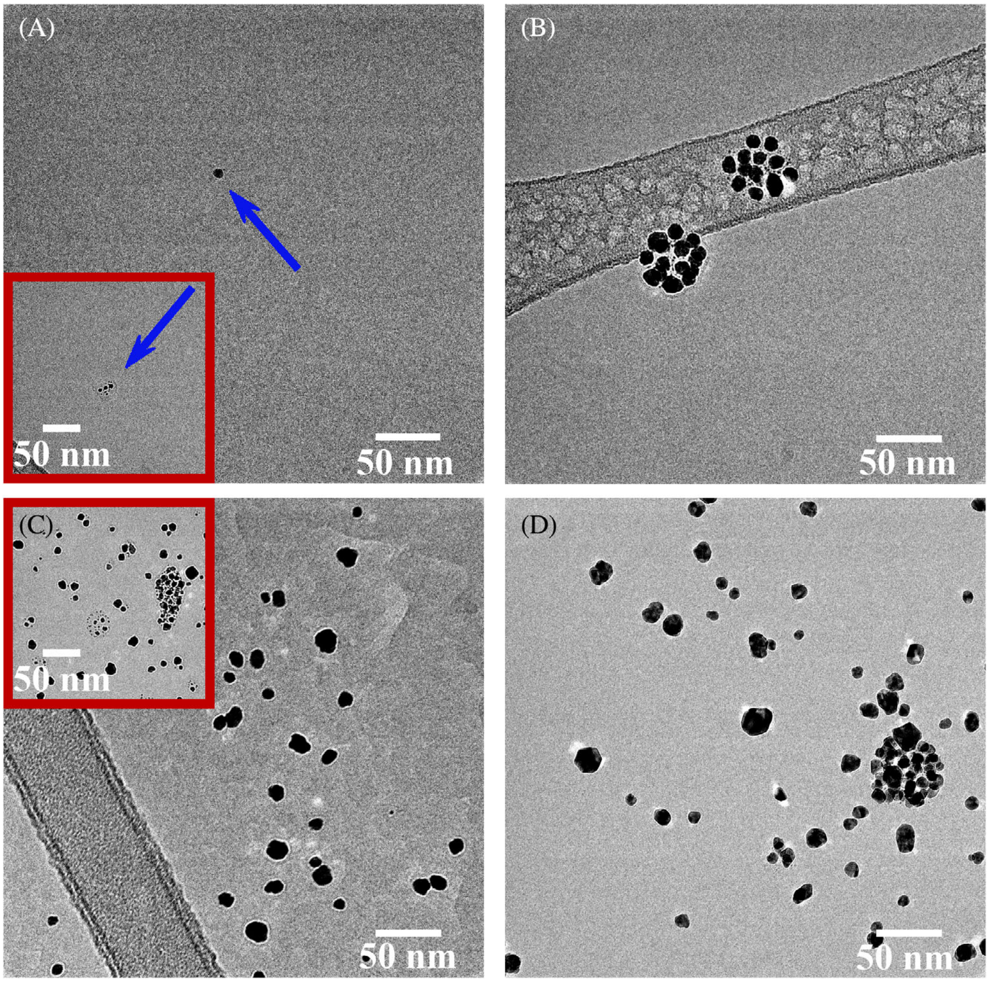

FIGURE 2 Cryo-TEM images of chitosan/silver dispersions of 1/0.10 (A,B) and 1/1.04 (C,D) composition at 1 day (A,C) and at 7 day (B,D) after heating at 60°C. The insets in (A) and (C) show agglomerates of nanoparticles. Blue arrows at (a) indicate the particles

both the nucleation of new nanoparticles and the reduction of silver directly under the action of an electron beam.[62] Figure 2B,D represent corresponding solutions at day 7 after preparation. The appearance of raspberry-like aggregates along with individual particles is observed for both chitosan to silver ratios. At the same time, there are significantly fewer individual particles in a solution with a low silver content. Therefore, based on the data of UV-spectroscopy and cryo-TEM, the formation of highly porous particles was carried out on the fifth day after the solutions preparation to avoid the formation of a large number of aggregates and to obtain a more homogeneous distribution of silver nanoparticles in the chitosan matrix.

Thus, four types of polymer particles differing in silver content were obtained. Particle morphology was studied by SEM. Figure 3A–D shows typical micrographs of particles depending on the composition. The images show the formation of a highly porous polymer framework, typical for all compositions. However, several features can be distinguished. Thus, at a low concentration of silver nitrate in the initial solution, a more "loose" fullerene-like structure with a large number of micron-sized pores is formed (Figure 3A,B). The structure of chitosan particles becomes denser with an increase of silver content in the stock liquid, and contains a larger number of pores, but smaller in size (Figure 3C,D). The average particle size, regardless of the composition, was about 116 ± 15 μm. The value exceeds the sizes of previously obtained particles of pure chitosan by almost two times. Such changes may be associated with the hydrolysis of chitosan due to keeping the acidic solution at an elevated temperature leading to a decrease in polymer molecular mass and, as a consequence, a change in viscosity.[63] In turn, a decrease in the viscosity is reflected in an increase in the consumption of the solution during spraying and an increase in the droplet size. So indeed, the viscosity of a 1 wt% solution of chitosan in 2 wt% acetic acid decreases exactly two times after thermostating at 60°C for 5 days (compare 8 and 4 mPa s, respectively). Additionally, the filler particles were subjected to elemental analysis. The experimental values correlate quite well with the calculated ones. Thus, it can be concluded that almost all silver passed from solution into particles. The observed differences in the structure of chitosan particles are also reflected in the bulk density (Table 1). The bulk density increases with silver content. At the same time, it is curious to note that for particles of composition 1/0.10 and 1/0.21, the values turn out to be lower than for pure highly porous chitosan particles.[43] A possible reason for the structural alterations observed in Figure 3 is the different mechanism of droplets crystallization in the process of spraying during the formation of particles. According to the study by Kiani et al.[64] at a high freezing rate, the number of primary nucleation centers is directly proportional to the concentration of particles in solution, that is, silver nanoparticles

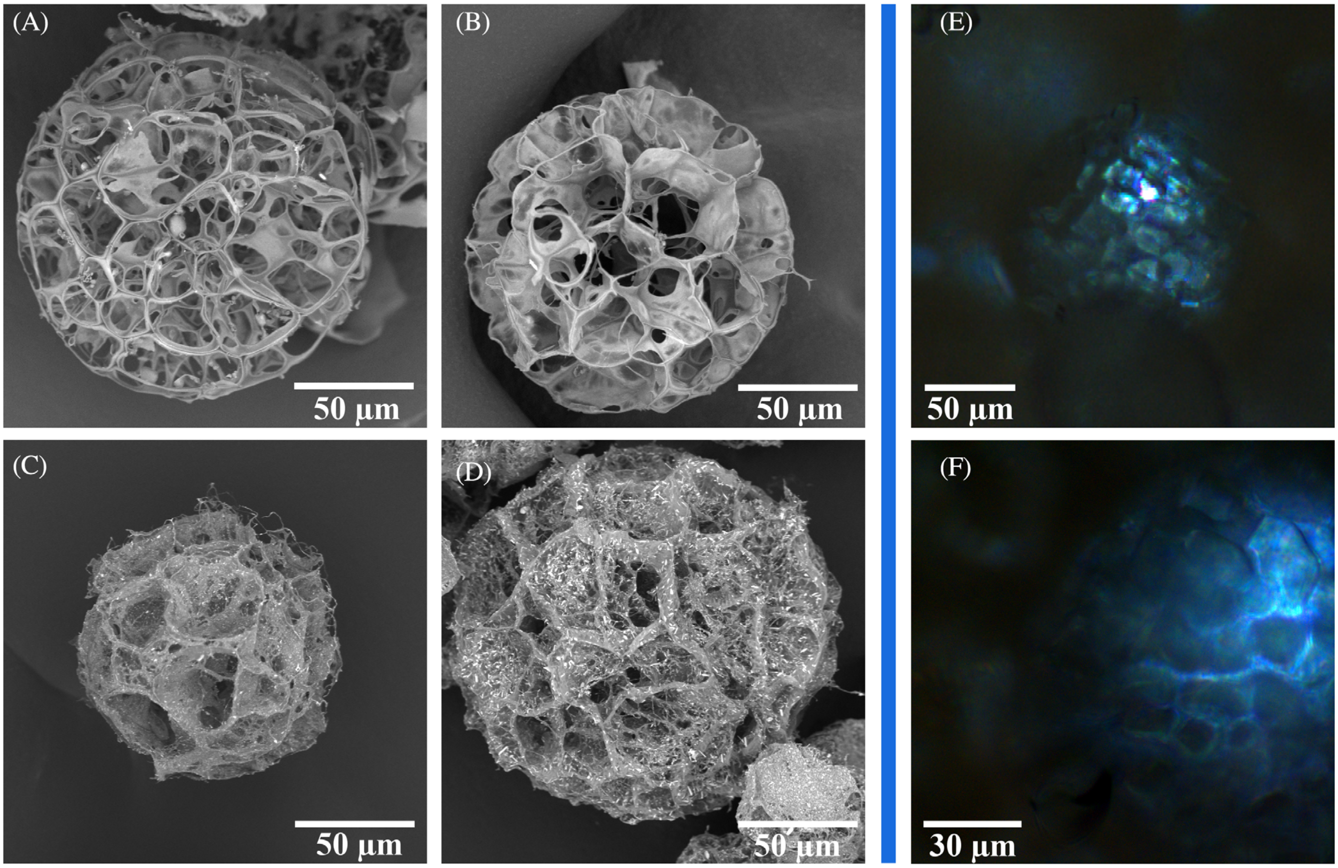

FIGURE 3 SEM images of porous chitosan particles doped by silver nanoparticles of 1/0.10 (A), 1/0.21 (B), 1/0.52 (C) and 1/1.04 (D) composition. Typical optical microscopy images in crossed polaroids of frozen particles at various magnifications (E, F)

TABLE 1 The silver content and bulk density of highly porous chitosan particles depending on the composition

Particles composition	1/0.10	1/0.21	1/0.52	1/1.04
Estimated silver content (wt%)	5.78	11.05	21.72	32.39
Measured silver content (wt%)	6.6 ± 0.5	11.9 ± 2.6	16.7 ± 1.4	36.5 ± 2.2
Bulk density (g/cm^3)	0.004	0.004	0.007	0.011

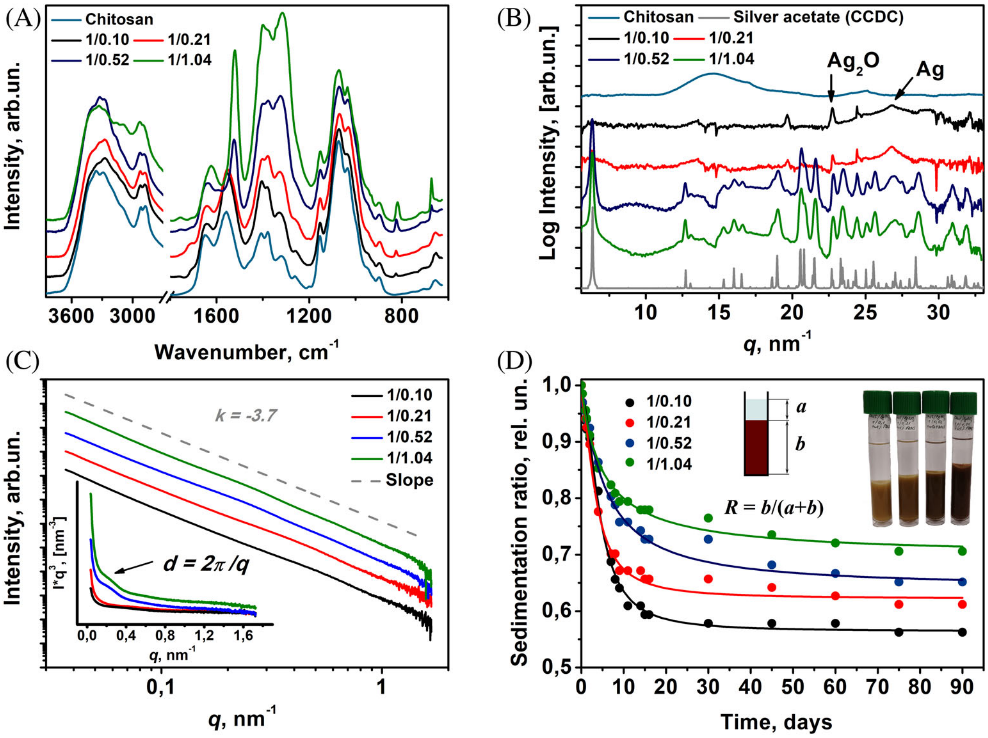

FIGURE 4 FTIR spectra (A), WAXS (B) and SAXS (C) curves of porous chitosan particles doped by various content of silver nanoparticles. The curves are shifted along intensity axis for clarity. The inset in (C) is Ruhland–Kratky plot. (D) The sedimentation ratio as function of time for 1 wt% suspensions of porous chitosan particles doped by various content of silver nanoparticles in silicon oil. The solid lines are a guide to the eye. The inset in (D) shows photograph of the samples after sedimentation test

in our case. Thus, the fewer nanoparticles in the solution, the fewer crystallization centers, and the larger the solvent crystallites formed and, as a result, the looser structure of porous chitosan particles. Optical microscopy images of frozen particles (Figure 3E,F) clearly show the formation of a cellular structure and microphase separation of the solution components inside the particle. Thus, solvent crystals are formed during freezing leading to the segregation of the polymer and nanoparticles with the formation of dense walls. It can be seen that the grain sizes correlate well with the macropore size in the freeze-dried particles.

FTIR spectroscopy provides valuable information about chemical composition of filler particles (Figure 4A). In the IR spectrum of pure chitosan particles, a broad absorption band is observed in the region of 3600–3000 cm^{-1} with peaks at 3359 and 3292 cm^{-1} and a shoulder in the region of higher wavenumbers, formed because of the overlapping of N—H and O—H stretching vibrations. Absorption bands at 2920 and 2875 cm^{-1} correspond to C—H stretching vibrations of bonds in the methylene groups (antisymmetric and symmetric, respectively), bands at 1379 and 1409 cm^{-1} are C—H bending vibrations and band at 899 cm^{-1} is attributed to the C—H bending out of the plane of the ring typical for monosaccharides. The absorption bands at 1651, 1557, and 1321 cm^{-1} are called Amide I (C=O stretching), Amide II (N—H bending and C—N stretching) and Amide III (C—N stretching), while a wide band with a maximum in the region of 3090 cm^{-1} is the overtone of the Amide II. The band at 1154 cm^{-1} corresponds to the stretching vibrations of the C—O—C bridges in the pyranose ring, and the peaks at 1073 and 1035 cm^{-1} correspond to the C—O stretching.[65]

During the reaction of chitosan with silver ion, the latter is reduced to silver, which can interact with the functional groups of the polymer. Therefore, noticeable changes in the IR spectra of composite particles are observed. Thus, the Amide I and II bands shift toward lower wavenumbers indicating the interaction of silver nanoparticles with the NH$_2$ groups of chitosan,[27,66] while the position of the absorption bands C—O and C—O—C does not undergo significant changes. In addition, as the silver content in the samples increases, there is a noticeable increase in intensity of the absorption bands in the region of 1550–1300 cm^{-1}. An increase in the intensity of these absorption bands may be associated with the appearance of stretching vibrations (antisymmetric at ~1520 cm^{-1} and symmetric at ~1390 cm^{-1}) of the carboxylate anion, which may indicate the formation of silver acetate, due to interaction of silver with acetic acid.[67] Moreover, a new band appears at 1756 cm^{-1} attributed to the absorption of carbonyl groups formed during the oxidation of the hydroxyl group of the monosaccharide link.[27] Another new band in the region of 825–820 cm^{-1} can be related with the absorption of the NO_3^- as a residual ion from silver salt.[68] The bands at 678 and 618 cm^{-1} can be attributed to vibrations of the Ag–O of silver oxide[69,70] possibly forming during the reduction of silver nitrate. It is obvious that the intensity of these bands increases with the content of silver in the particles. Thus, the IR spectra confirm the formation of Ag-containing composite particles.

To determine the crystal structure of nanosilver-chitosan composites X-ray diffraction experiments were carried out in wide angle transmission setup. While the initial chitosan matrix is amorphous, formation of even low amounts of silver nanoparticles results in appearance of low intensity crystalline reflections of silver and its oxides (Figure 4B). Thus, the data confirm the recovery of silver from solution and the formation of silver-containing nanoparticles. Increasing the chitosan to silver ratio higher to 1/0.52 led to drastic changes in diffraction pattern, showing a set of a rather sharp reflections. This pattern was mostly attributed to silver acetate, crystal pattern of which is shown for comparison. The crystallite size estimated from Scherrer equation was roughly 40 nm. Apparently, the amount of chitosan is high enough to coordinate most of the ions at a low silver content in the solution. With an increase in the silver content, some of the ions remain in the solution in the form of weakly bound acetate, which crystallizes when the solution is sprayed into liquid nitrogen. The result obtained is extremely important, because it determines the coordinating ability of chitosan. Note that the intensity of the silver nanoparticles pattern also increases with concentration against the background of silver acetate patterns. Thus, depending on the composition of the stock solution, composite particles of highly porous chitosan doped with silver-containing nanoparticles of various nature were obtained.

SAXS method is a promising tool for analyzing the structural organization of nanoscale objects. Figure 4C shows SAXS curves for filler powders of various composition. An extended linear section in double logarithmic scale indicates the fractal structure of the scattering object and makes it possible to evaluate the morphology of polymer walls surface. The slope (k) is close to -3.7 well correlating with previously obtained result for pure porous chitosan particles and indicating the surface type of the fractal with dimension of 2.3.[43] The value of 2.3 is typical for a fairly smooth surface with small roughness corresponding to chitosan segregation into the macropore walls due to the crystallization of the solvent during freezing. Moreover, a weakly expressed maximum appears on the curves in the region of 0.15–0.40 nm^{-1} with an increase in the silver content in the filler composition, which is more pronounced in Ruhland–Kratky plot (the inset Figure 4C). Obviously, the maximum associated with the inclusion of silver-containing nanoparticles, both pure silver and acetate, in the structure of the polymer walls. Note that the intensity of the maximum increases with increasing silver to chitosan ratio. Valuable information can be obtained from the position of this maximum to determine the distance $d \approx 25$ nm between scattering objects.

One of the most important properties of any suspension is sedimentation stability reflecting the possibility of the material long-term use. If the viscosity of the dispersion medium is relatively high, the sedimentation process is typically prolonged in time and takes hours, days, and even months. Therefore, the stability of fluids is typically evaluated by the final sedimentation ratio and by the time it takes to reach it. Figure 4D shows the dependences of the sedimentation ratio for 1 wt% suspensions filled with particles of various composition. It can be seen that the sedimentation ratio reaches a constant value during about a month for all samples. The value of the final sedimentation ratio is associated with the process of colloidal structure formation from interacting filler particles and is primarily determined by the volume fraction and density of the filler. A significant level of the equilibrium colloidal phase was previously explained by the blotting of highly porous particles and the penetration of dispersion media molecules into macropores. It is surprising that the value of the final sedimentation ratio increases with an increase in the ratio of silver to chitosan in the particles composition, since the proportion of chitosan, and hence the number of porous particles, decreases. Indeed, the more silver in the composition of the particles, the greater weight the particles and the smaller the number of particles contained in 1 wt% suspension. Such unusual behavior can be explained quite trivially, namely by the different structure of the used particles (Figure 3). Thus, a looser polymer framework of particles at 1/0.10 and 1/0.21 composition leads to a more significant compaction of particles during the formation of the equilibrium colloidal structure compared to a denser structure of particles at 1/0.52 and 1/1.04 composition.

Such differences in particle structure should be reflected in the rheological behavior of suspensions without and under electric field. The shear stress increases with increasing shear rate for all samples. The yield curves coincide at shear rate above 10 s^{-1}, the values increase linearly, and the samples exhibit Newtonian behavior (Figure 5A). That is, in this shear rate range, the colloidal structure of the suspension is destroyed and the properties of the fluid are mainly determined by the properties of the dispersion medium. At lower shear rates, a deviation from the linear dependence is observed, and the nature of flow changes. Note the similarity of the curves for suspensions containing particles of 1/0.10 and 1/0.21 as well as 1/0.52 and 1/1.04 composition, which correlates with the SEM data (Figure 3). Shear stress values at low shear rate are higher for suspensions with a high silver content indicating a more elastic response of the material. Such effect is caused by a denser structure of the porous filler particles with higher silver to chitosan ratio.

The behavior of the samples changes under an electric field. Figure 5B shows the yield curves at various electric field strengths for 1/1.04 sample, as an example. Similar dependencies are typical for all studied fluids, but to a much lesser extent. A plateau appears on the flow curves in the region of low shear rates (< 30 s^{-1}) and the shear stress values increase with an increase in the electric field strength by several orders of magnitude. Thus, yield stress is revealed and transition from viscous to solid-like behavior occurs. The transition is caused by the polarization of the dispersed phase particles and the formation of columnar structures, which are destroyed during the shear flow. The data shown in Figure 5B were obtained in the CSR mode, so during the measurement process, a continuous breakdown-recovery of the colloidal structure occurs, and the magnitude of the shear stress is determined by the balance of polarization and shear

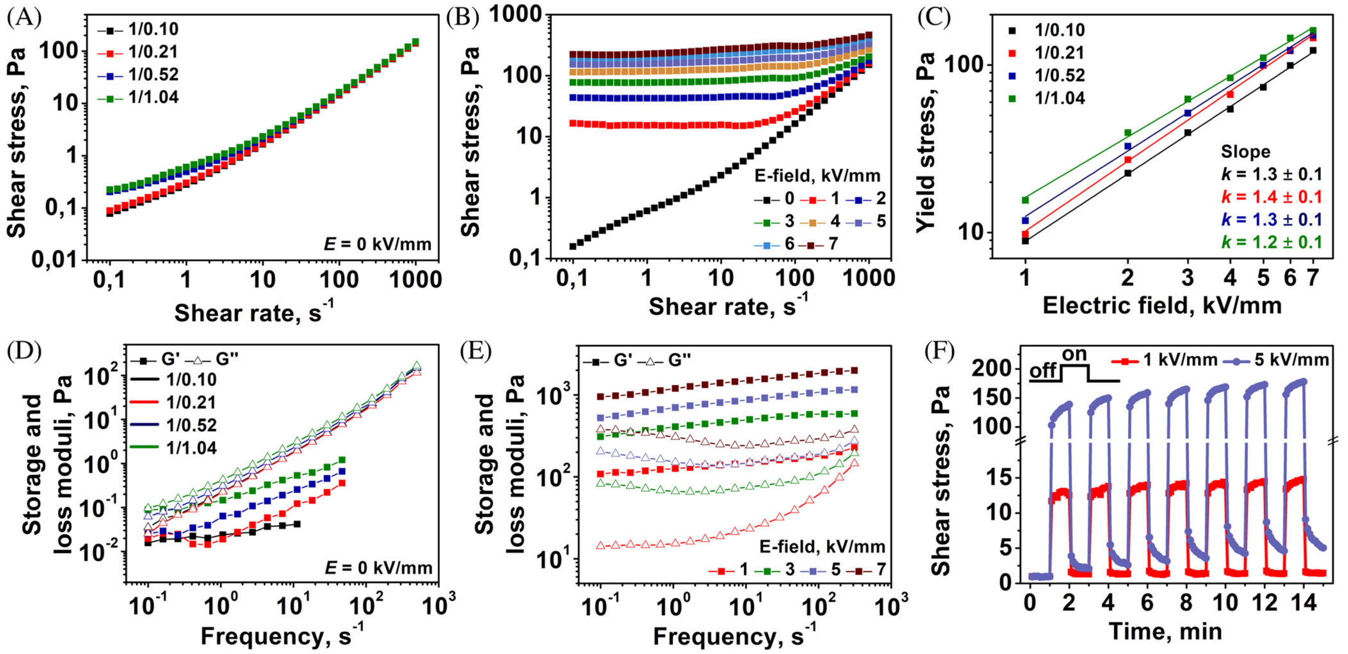

FIGURE 5 (A) Flow curves of 1 wt% PDMS suspensions filled with porous chitosan particles doped by silver nanoparticles of 1/0.10, 1/0.21, 1/0.52 and 1/1.04 composition. (B) Flow curves of 1 wt% PDMS suspensions filled with particles of 1/1.04 composition at various electric field strength. (C) Static yield stress as function of electric field strength for 1 wt% PDMS suspensions filled with porous chitosan particles with various silver content. The slope corresponds t the mechanism of electrorheological effect. (D) Frequency dependencies of storage and loss moduli of studied suspensions. (E) Typical changes of moduli under electric field for suspension filled with particles of 1/1.04 composition at several electric field strength. All data in (D, E) were obtained at the value of strain in linear viscoelastic range. (F) Shear stress as function of time for 1 wt% PDMS suspensions filled with particles of 1/1.04 composition under switching electric field. Data were obtained in CSR mode at low shear rate of 1 s^{-1}

forces.[71] The values of the shear stress rise with a significant increase in the shear rate, the shear forces prevail, and eventually the flow curves tend to grow linearly. This is the case when the structure is completely destroyed and cannot be restored by the electric field. Note that the value of the shear rate corresponding the transition to the shear forces domination increases with an electric field. Figure 5C shows the dependences of the static yield stress on the electric field strength for all the studied ERFs in double logarithmic scale. An increase in values is observed both with the electric field strength and with the silver nanoparticles content in the filler composition. The slope of corresponding dependencies designates the mechanism of electrorheological effect. The value of two is typical for traditional fluids indicating only the polarization nature of the effect and decreases down to one for mechanism of saturated polarization. For ERFs under study, the slope of dependencies weakly depends on filler particles composition and varies in the range of 1.2–1.4 corresponding to complicated mechanism involving conductivity along with polarization.[72] Such result matches with the previously obtained data for suspensions of pure porous chitosan particles[43] and shows that silver nanoparticles doping does not affect the nature of electrorheological response. The corresponding values of the current density during rheological measurements are shown in Figure S1. As expected, the current density increases with an increase in the electric field strength and the silver content in the composite filler composition. However, the values are relatively low and do not exceed 4 μA cm^{-2}.

The contrast of the change in the rheological behavior of the ERFs in an electric field can be comprehended by relative efficiency:

$$\mathrm{Eff}_{\mathrm{rel.}} = ((\tau_E - \tau_0)/\tau_0) \quad (1)$$

where Eff$_{\mathrm{rel.}}$ is relative efficiency, τ_E is the yield stress of the ERF at given electric field strength, τ_0 is typically the yield stress at zero electric field or shear stress at low shear rate of 0.1 s^{-1}. Such assessment can be rather ambiguous for fluids without yield stress at zero electric field because of uncertainty in τ_0 value, but allows qualitatively analyze the fluid response. The values of the relative efficiency of ERFs filled with particles of various composition are summarized in Table 2.

The relative efficiency of ERFs increases with electric field strength showing higher elastic response. Note the nonlinear change in the relative efficiency of samples with increasing silver content. The highest values were obtained for the fluid filled with particles of 1/0.21 composition at all studied electric field strengths. A significant decrease in the relative efficiency is observed (more than two times) with an increase in the ratio of silver to chitosan. Two factors lead to this effect. The first one is a looser particle structure (Figure 3), which results in a weak visco-elastic response of suspension out-of-field at studied concentration (Figure 5A). Another one is a proper balance of

TABLE 2 Relative efficiency of ERFs filled with particles of various composition

Filler	Relative efficiency (rel. un.)			
E (kV mm^{-1})	1/0.10	1/0.21	1/0.52	1/1.04
1	104	112	54	71
2	265	313	151	182
3	465	595	239	290
4	642	768	389	389
5	867	1147	462	512
6	1171	1401	567	672
7	1441	1672	698	746

Notes: The static yield stress data were used for analysis.

chitosan to silver resulting in full coordination of silver ions and absence of superfluous silver acetate providing better particle polarization and the formation of stronger structures in electric field.

The frequency dependences of the storage and loss moduli confirm the results obtained in shear experiments. Thus, at zero electric field, all samples show a viscous response: the values of the loss modulus are higher than the storage modulus. The values of the loss modulus increase with frequency, but weakly depend on the composition of the filler particles. A trend toward an increase in the values with an increase of the silver nanoparticles content in the filler can be identified, which is consistent with the volumetric filling degree of fluids. Note that the storage modulus is detected only at low frequencies (less than 50 s^{-1}) and its values rise with the content of silver nanoparticles in the filler. Such behavior confirms the increase in the elastic response of fluids with a change in the filler composition and the formation of denser particles at a high chitosan to silver ratio of 1/0.52 and 1/1.04. The storage modulus exceeds the loss modulus under an electric field in the entire studied frequency range. Moreover, the values of both moduli increase with increasing electric field strength. The structure formed under an electric field becomes more elastic. The results confirm the yield stress and the solid-like behavior of the ERFs under an electric field. An important property of ERF characterizing the possibility of its practical application is a stable response in the on/off mode, which determines the stability of the material cyclic operation. Figure 5F shows typical dependences of the shear stress over time under switching electric field at low (1 kV mm^{-1}) and high (5 kV mm^{-1}) strengths. When the field is turned on, a sharp jump in the shear stress is observed with a corresponding rapid relaxation when the potential is removed. It is important to note that, regardless of the field strength, there is a slight increase in values over time. We note the hysteresis of properties during relaxation and the duration of the process in time at a high field strength. When the electric field is removed, the residual shear stress after several cycles is about 5 Pa indicating the structure relaxation not to individual particles, but to secondary aggregates, which are then polarized as a whole and form the percolation structure faster. Nevertheless, with an increase in the relaxation time, the behavior of the suspensions return to the original level. Data clearly show the possibility of cyclic operation and show reversible and reproducible performance of ERFs even at high electric fields.

Important information about the nature of electrorheological effect as well as the explanation of the differences in rheological behavior of suspensions can be provided by dielectric spectroscopy studies.[73,74] Figure 6A–C displays the frequency dependence of conductivity, dielectric permittivity and loss factor for studied ERFs at 20 °C. The values of conductivity, dielectric losses and polarizability increase non-linearly with increasing silver content. Thus, the low-frequency conductivity increases by 20% with an increase in chitosan to silver ratio from 1/0.10 to 1/0.52, and then increases by almost 300% at a concentration of 1/1.04, which indicates an approach to the percolation threshold of silver-contain nanoparticles in porous chitosan filler. All the fluids show obvious dielectric relaxation peaks within the measured frequency range. Two relaxation processes can be distinguished on the presented dielectric spectra. Owing to the fact that the relative permittivity of insulating dispersion media liquid is nearly independent of frequency and the loss factor is two orders of magnitude lower than in the studied spectra within the measured range, the observed dielectric relaxation peaks is caused by the polarization process of filler particles. The dielectric loss peak of the first one is in the kilohertz region of the spectra. Such relaxations are observed in a variety of ERFs and typically associated with filler particle polarization. The second relaxation process has a not-resolved loss peak in the low-frequency region beyond the measurement range. Typically, the electrode polarization means the development of ionic double layers formed by ions migrated toward the electrode/sample interface. The presence of a thin layer of insulating PDMS between the metallic electrode and the sample leads to the impossibility for steady- and low-frequency current to flow and to the accumulation of space charge within the sample. Thus, observed relaxation process corresponds to the polarization of the entire ERF sample, that is, colloidal structure formed by porous particles.

It is important to note that the polarization and relaxation of silver nanoparticles is an extremely fast process. It should be observed in the region of very high frequencies and is outside the measurement range as well. Thus, we cannot distinguish the polarization of nanoparticles in the structure of a porous polymer filler, but we can analyze the effects associated with the influence of silver on the polarization of the filler as a whole. In order to separate two observed overlapping relaxation processes and provide a quantitative analysis, the dielectric spectra were deconvoluted by the combination of two Cole-Cole relaxations and a DC conductivity terms:

$$\varepsilon^* = \varepsilon_\infty + \frac{\Delta\varepsilon_1}{1+(i\omega\tau_1)^{\beta_1}} + \frac{\Delta\varepsilon_2}{1+(i\omega\tau_2)^{\beta_2}} + i\frac{\sigma_{dc}}{\varepsilon_0\omega} \tag{2}$$

where $\Delta\varepsilon = \varepsilon_s - \varepsilon_\infty$ is the dielectric relaxation strength, ε_s and ε_∞ is the limit values of the relative permittivity at the frequencies below and above the relaxation frequencies, respectively, ε_s is the static permittivity, $\omega = 2\pi f$ (s^{-1}) is the angular frequency and τ (s) is the characteristic dielectric relaxation time of the process. Exponent β ($0 < \beta \leq 1$) defines the measure of the relaxation time distribution associated with particles and their clusters (β_1 and β_2, respectively), i.e. broadness of the corresponding spectra, σ ($S\,m^{-1}$) is the DC conductivity, ε_0 ($F\,m^{-1}$) – electric constant.

Two deconvoluted dispersion spectra of 1/1.04 sample are shown in the Figure 6D as an example. Cole–Cole plot in the inset clearly demonstrates the contribution of corresponding relaxation processes. The relaxation peak in the kilohertz region is revealed for all samples and is especially well expressed for suspension filled with particles of 1/1.04 composition. However, such peak was not previously detected for fluids filled with undoped porous chitosan particles,[43] which seems to indicate significantly increased polarization of silver-containing particles and affects the electrorheological activity of the filler. According to the proposed electrorheological mechanism, the polarization rate of particles is important for maintaining chain-like structures formed by particles dispersed in oil under a simultaneous influence of both electric and shearing fields. Thus, the relaxation time of the 10^{-3}–10^{-6} s as well as high dielectric relaxation strength is required for a high electrorheological effect. Too low relaxation time cannot result in adequate particle polarization during flow, while too high relaxation time may turn into repulsive interaction between particles.[75] As one can see from the figure, a suspension with the composition of 1/1.04 has the most preferred electrophysical parameters at room and higher temperatures. An increase of silver content increases the dielectric relaxation strength $\Delta\varepsilon$ of the individual particles (2nd process) from 1.1 to 1.9, which is a substantial growth.

The dielectric loss peaks for suspensions shift to the short-wavelength region of the spectrum with temperature due to thermal

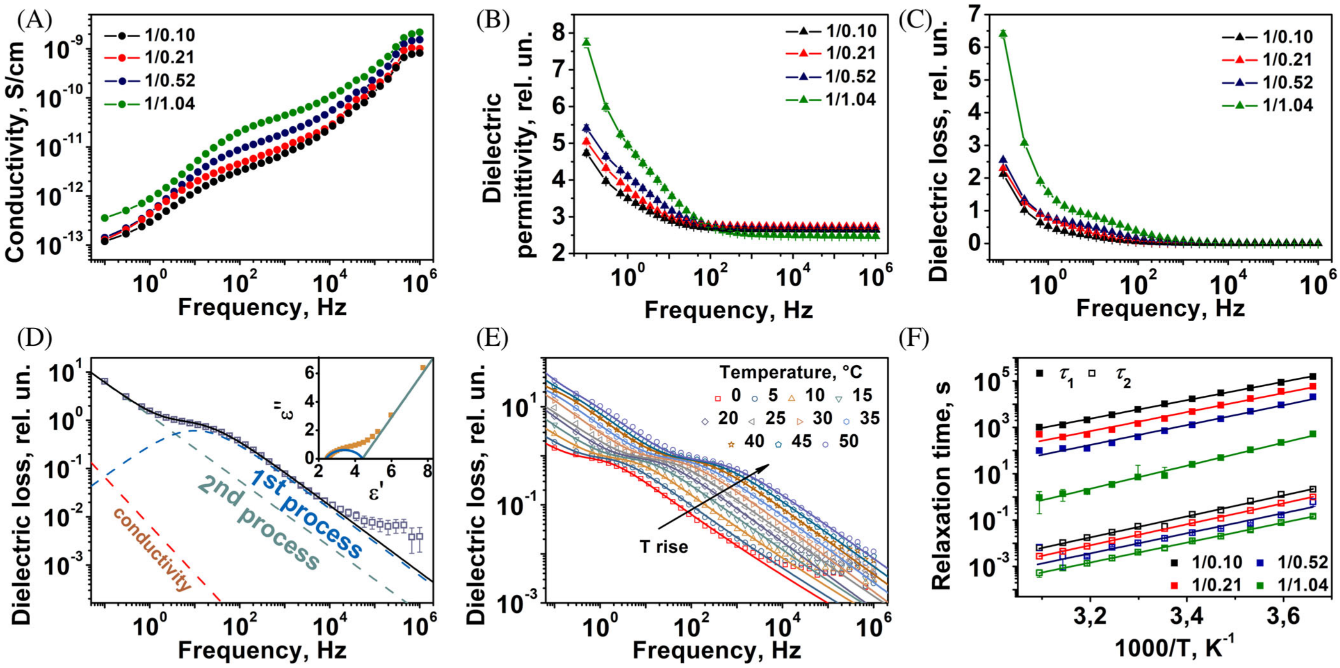

FIGURE 6 Frequency dependence of conductivity (A), dielectric permittivity (B) and loss factor (C), for suspensions filled with porous chitosan particles doped by silver nanoparticles of 1/0.10, 1/0.21, 1/0.52 and 1/1.04 composition. (D) Deconvoluted plot ε'' versus f. The inset depicts the Cole–Cole diagram of presented spectra. The dashed lines illustrate the contribution from each separate dispersion to the total fit. (E) Frequency dependence of the dielectric loss at various temperatures of 1/1.04 suspension. (F) The relaxation time as a function of reciprocal temperature

TABLE 3 Parameter values for the Arrhenius-type dependence of relaxation time of the 1st and 2nd processes

Filler composition	1/0.10	1/0.21	1/0.52	1/1.04
1st process E_a (kJ mol^{-1})	33 ± 1	34 ± 1	36 ± 2	41.3 ± 0.4
2nd process E_a (kJ mol^{-1})	38 ± 1	37.2 ± 0.3	33 ± 1	35.7 ± 0.3

activation of the relaxation process (Figure 6E). The plot of average relaxation time, calculated by fitting the data by Equation 2, as a function of reciprocal temperature $\tau = f\left(1000\,T^{-1}\right)$ is shown in Figure 6F. Increasing silver content leads to an almost proportional rise of the relaxation strength and decrease of activation energy. Thus, the temperature dependence of the relaxation process for all the samples can be described by the Arrhenius equation:

$$\tau = \tau_0 e^{\frac{E_a}{RT}} \tag{3}$$

where E_a (J mol^{-1}) is the activation energy, R (J·K^{-1}·mol^{-1}) is the gas constant, and T (K) is the absolute temperature.

The E_a values calculated by the slope on the 1000 T^{-1} coordinate are shown in the Table 3. This Arrhenius-type temperature dependence and the magnitude of the activation energies suggest Maxwell–Wagner polarization of particles driven by electron hopping mechanism rather than ionic transport, generally influenced by molecular mobility. The activation energy of σ-relaxation associated with the hopping motion of ions in the disordered structure for chitosan usually exceed 80 kJ mol^{-1}.[76] Therefore, it can be assumed that the inclusion of silver nanoparticles increases the polarizability of porous filler particles and affects the electrorheological properties of the studied fluids.

4 | CONCLUSION

The role of silver dopant on the electrorheological properties of porous chitosan particles suspensions in silicon oil has been revealed. A study of the silver recovery from solution by chitosan showed a significant effect of the components ratio on the nanoparticles growth. When the chitosan to silver ratio is less than 1/0.21 by weight, the number of chitosan units is high enough for almost complete coordination of silver ions. However, some of the ions remain in solution with an increase in the silver content leading to additional crystallization of silver acetate during the formation of highly porous particles by spraying into liquid nitrogen. During the reduction of silver ions by chitosan, the growth of individual nanoparticles is observed accompanied by aggregation in long term with the formation of raspberry-like particles. The effect of the stock solution viscosity on the size of the formed highly porous filler particles was found. The viscosity decrease is caused by a drop in the molecular weight of chitosan due to acidic hydrolysis at elevated temperature. An approach has been proposed for the creation of in situ silver-doped highly porous particles exhibiting increased electrorheological activity. The suspensions of polymer filler particles in silicon oil reveal a pronounced electrorheological effect under electric field at low concentration of 1 wt%. The intensity of the effect increases with increasing silver content and is determined by the electrophysical characteristics of suspensions. The studied ERFs show suitable sedimentation stability and a stable response under switching electric field. The yield stress of developed ERFs under electric field is comparable with compositions at a filler content an order of magnitude higher, which can reduce the cost of the material. The prospects of creating hybrid composite fillers to affect the properties of ERFs have been confirmed. Thus, it is possible to control the relative efficiency of the material and obtain fluids with a more contrasting transition from a viscous state to an elastic one by adjusting the filler structure.

ACKNOWLEDGMENTS

This work was partially funded by Russian Science Foundation (project no. 20-73-00205). Analysis of the purity of the materials used in this work were supported by the Ministry of Science and Higher Education of the Russian Federation (Contract FFSM-2021-0005). The authors thank the resource centers for organic and hybrid materials “Polymer”, probe and electron microscopy “Nanozond”, as well as optical microscopy and spectroscopy “Optics” of the National Research Center “Kurchatov Institute” for the opportunity to carry out the measurements. The analysis of the molecular-weight characteristics of PDMS was performed at the Collaborative Access Center “Center for Polymer Research” of the Enikolopov Institute of Synthetic Polymeric Materials, Russian Academy of Sciences.

DATA AVAILABILITY STATEMENT

The data that support the findings of this study are available from the corresponding author upon reasonable request.

ORCID

Nikita M. Kuznetsov https://orcid.org/0000-0002-1241-3115
Victoria V. Kovaleva https://orcid.org/0000-0002-4137-7758
Danila A. Volkov https://orcid.org/0000-0003-3506-5595
Yuriy D. Zagoskin https://orcid.org/0000-0002-5825-8333
Artem Yu. Vdovichenko https://orcid.org/0000-0002-0099-6202
Sergey N. Malakhov https://orcid.org/0000-0002-9015-2117
Artem V. Bakirov https://orcid.org/0000-0003-0798-2791
Eugeny V. Yastremsky https://orcid.org/0000-0002-3183-7060
Roman A. Kamyshinsky https://orcid.org/0000-0002-8546-7763
Alexei A. Stupnikov https://orcid.org/0000-0003-1711-9756
Sergei N. Chvalun https://orcid.org/0000-0001-9405-4509
Timofei E. Grigoriev https://orcid.org/0000-0001-8197-0188

REFERENCES

1. Majeti NV, Kumar R. A review of chitin and chitosan applications. *React Funct Polym*. 2000;46:1-27.
2. Foster LJR, Ho S, Hook J, Basuki M, Marçal H. Chitosan as a biomaterial: influence of degree of deacetylation on its physiochemical, material and biological properties. *PLoS One*. 2015;10(8):1-22. doi:10.1371/journal.pone.0135153
3. Francis Suh JK, Matthew HWT. Application of chitosan-based polysaccharide biomaterials in cartilage tissue engineering: a review. *Biomaterials*. 2000;21(24):2589-2598. doi:10.1016/S0142-9612(00)00126-5
4. Helander IM, Nurmiaho-Lassila EL, Ahvenainen R, Rhoades J, Roller S. Chitosan disrupts the barrier properties of the outer membrane of gram-negative bacteria. *Int J Food Microbiol*. 2001;71(2–3):235-244. doi:10.1016/S0168-1605(01)00609-2
5. Park PJ, Je JY, Kim SK. Free radical scavenging activities of differently deacetylated chitosans using an ESR spectrometer. *Carbohydr Polym*. 2004;55(1):17-22. doi:10.1016/j.carbpol.2003.05.002

6. Kalantari K, Afifi AM, Jahangirian H, Webster TJ. Biomedical applications of chitosan electrospun nanofibers as a green polymer – review. *Carbohydr Polym*. 2019;207:588-600. doi:10.1016/j.carbpol.2018.12.011
7. Dash M, Chiellini F, Ottenbrite RM, Chiellini E. Chitosan—a versatile semi-synthetic polymer in biomedical applications. *Prog Polym Sci*. 2011;36(8):981-1014. doi:10.1016/j.progpolymsci.2011.02.001
8. Moura D, Mano JF, Paiva MC, Alves NM. Chitosan nanocomposites based on distinct inorganic fillers for biomedical applications. *Sci Technol Adv Mater*. 2016;17(1):626-643. doi:10.1080/14686996.2016.1229104
9. Sadasivuni KK, Ponnamma D, Kim J, Cabibihan JJ, MA AM, eds. *Biopolymer Composites in Electronics*. Elsevier Inc; 2017. doi:10.1016/C2014-0-04575-3
10. Bazargan G, Fischer SA, Gunlycke D. Quantifying proton diffusion in acid-functionalized chitosan membranes. *Comput Mater Sci*. 2022;210:110988. doi:10.1016/j.commatsci.2021.110988
11. Du L, Li T, Jin F, et al. Design of high conductive and piezoelectric poly (3,4-ethylenedioxythiophene)/chitosan nanofibers for enhancing cellular electrical stimulation. *J Colloid Interface Sci*. 2020;559:65-75. doi:10.1016/j.jcis.2019.10.003
12. Neagu AM, Curecheriu LP, Cazacu A, Mitoseriu L. Impedance analysis and tunability of $BaTiO_3$-chitosan composites: towards active dielectrics for flexible electronics. *Compos Part B Eng*. 2014;66:109-116. doi:10.1016/j.compositesb.2014.04.020
13. Ehsani A, Bigdeloo M, Assefi F, Kiamehr M, Alizadeh R. Ternary nanocomposite of conductive polymer/chitosan biopolymer/metal organic framework: synthesis, characterization and electrochemical performance as effective electrode materials in pseudocapacitors. *Inorg Chem Commun*. 2020;115:107885. doi:10.1016/j.inoche.2020.107885
14. Ko YG, Chun YJ, Kim JY, Choi US. Influence of metal ion on electrorheological properties of carboxyl-group-immobilized chitosan dispersed suspension under electric field. *Colloids Surf A Physicochem Eng Asp*. 2010;371(1–3):76-80. doi:10.1016/j.colsurfa.2010.09.006
15. Awwad NS, El-Kader MFHA, Ibrahium HA, Asnag GM, Morsi MA. Green synthesis of different ratios from bimetallic gold: silver nanoparticles core@shell via laser ablation scattered in chitosan-PVA matrix and its electrical conductivity behavior. *Compos Commun*. 2021;24:100678. doi:10.1016/j.coco.2021.100678
16. Peng K, Wang W, Zhang J, et al. Preparation of chitosan/sodium alginate conductive hydrogels with high salt contents and their application in flexible supercapacitors. *Carbohydr Polym*. 2022;278:118927. doi:10.1016/j.carbpol.2021.118927
17. Ling Y, Luo Y, Luo J, Wang X, Sun R. Novel antibacterial paper based on quaternized carboxymethyl chitosan/organic montmorillonite/ag NP nanocomposites. *Ind Crops Prod*. 2013;51:470-479. doi:10.1016/j.indcrop.2013.09.040
18. Baláž M, Daneu N, Balážová Ľ, et al. Bio-mechanochemical synthesis of silver nanoparticles with antibacterial activity. *Adv Powder Technol*. 2017;28(12):3307-3312. doi:10.1016/j.apt.2017.09.028
19. Dong Y, Zhu H, Shen Y, Zhang W, Zhang L. Antibacterial activity of silver nanoparticles of different particle size against vibrio Natriegens. *PLoS One*. 2019;14(9):1-12. doi:10.1371/journal.pone.0222322
20. Khatoon UT, Rao GVSN, Mantravadi KM, Oztekin Y. Strategies to synthesize various nanostructures of silver and their applications—a review. *RSC Adv*. 2018;8(35):19739-19753. doi:10.1039/c8ra00440d
21. Kim KS, Park BG, Kim H, Lee HS, Jung SB. Fabrication of ag-MWNT nanocomposite paste for high-power LED package. *Curr Appl Phys*. 2015;15(S1):S36-S41. doi:10.1016/j.cap.2015.03.006
22. Jung KH, Min KD, Lee CJ, et al. Effect of epoxy content in ag nanoparticle paste on the bonding strength of MLCC packages. *Appl Surf Sci*. 2019;495:143487. doi:10.1016/j.apsusc.2019.07.229
23. Keller P, Kawasaki H. Conductive leaf vein networks produced via ag nanoparticle self-assembly for potential applications of flexible sensor. *Mater Lett*. 2021;284:128937. doi:10.1016/j.matlet.2020.128937
24. Puente C, Sánchez-Domínguez M, Brosseau CL, López I. Silver-chitosan and gold-chitosan substrates for surface-enhanced Raman spectroscopy (SERS): effect of nanoparticle morphology on SERS performance. *Mater Chem Phys*. 2021;260:124107. doi:10.1016/j.matchemphys.2020.124107
25. Yoon S, Kim HK. Cost-effective stretchable ag nanoparticles electrodes fabrication by screen printing for wearable strain sensors. *Surf Coatings Technol*. 2020;384:125308. doi:10.1016/j.surfcoat.2019.125308
26. Barkat Rezaei Z, Rastegarzadeh S, Kiasat A. In-situ decorated silver nanoparticles on electrospun poly (vinyl alcohol)/chitosan nanofibers as a plasmonic sensor for azathioprine determination. *Colloids Surfaces A Physicochem Eng Asp*. 2018;559:266-274. doi:10.1016/j.colsurfa.2018.09.047
27. Wei D, Qian W. Facile synthesis of ag and au nanoparticles utilizing chitosan as a mediator agent. *Colloids Surfaces B Biointerfaces*. 2008;62(1):136-142. doi:10.1016/j.colsurfb.2007.09.030
28. Carapeto AP, Ferraria AM, do Rego AMB. Unraveling the reaction mechanism of silver ions reduction by chitosan from so far neglected spectroscopic features. *Carbohydr Polym*. 2017;174:601-609. doi:10.1016/j.carbpol.2017.06.100
29. Lu Q, Han WJ, Choi HJ. Smart and functional conducting polymers: application to electrorheological fluids. *Molecules*. 2018;23(11):2854. doi:10.3390/molecules23112854
30. Dong YZ, Choi K, Kwon SH, Do NJ, Choi HJ. Nanoparticles functionalized by conducting polymers and their electrorheological and magnetorheological applications. *Polymers*. 2020;12(1):204. doi:10.3390/polym12010204
31. Dong YZ, Seo Y, Choi HJ. Recent development of electro-responsive smart electrorheological fluids. *Soft Matter*. 2019;15(17):3473-3486. doi:10.1039/c9sm00210c
32. Ko YG, Shin SS, Choi US, Park YS, Woo JW. Gelation of chitin and chitosan dispersed suspensions under electric field: effect of degree of deacetylation. *ACS Appl Mater Interfaces*. 2011;3(4):1289-1298. doi:10.1021/am200091r
33. Yoon C-M, Jang Y, Noh J, Kim J, Lee K, Jang J. Enhanced electrorheological performance of mixed silica nanomaterial geometry. *ACS Appl Mater Interfaces*. 2017;9(41):36358-36367. doi:10.1021/acsami.7b08298
34. Stolyarova DY, Kuznetsov NM, Belousov SI, Chvalun SN. Electrorheological behavior of low filled suspensions of highly anisometric montmorillonite particles. *J Appl Polym Sci*. 2019;136(25):47678. doi:10.1002/app.47678
35. Yin J, Zhao X. Titanate nano-whisker electrorheological fluid with high suspended stability and ER activity. *Nanotechnology*. 2006;17(1):192-196. doi:10.1088/0957-4484/17/1/031
36. Yin J, Xia X, Xiang L, Zhao X. Conductivity and polarization of carbonaceous nanotubes derived from polyaniline nanotubes and their electrorheology when dispersed in silicone oil. *Carbon*. 2010;48(10):2958-2967. doi:10.1016/j.carbon.2010.04.035
37. Rozynek Z, Silva SM L, Fossum JO, et al. Organoclay polypropylene nanocomposites under different electric field strengths. *Appl Clay Sci* 2014;96:67–72. doi:10.1016/j.clay.2014.03.011
38. Wang J, Zhao X, Liu Y, et al. Small-angle X-ray scattering study on the orientation of suspended sodium titanate nanofiber induced by applied electric field. *Radiat Detect Technol Methods*. 2019;36:1-7. doi:10.1007/s41605-019-0118-y
39. Kuznetsov NM, Bakirov AV, Banin EP, Belousov SI, Chvalun SN. In situ X-ray analysis of montmorillonite suspensions in polydimethylsiloxane: orientation in shear and electric field. *Colloids Surfaces A*

Physicochem Eng Asp. 2021;622:126663. doi:10.1016/j.colsurfa.2021.126663

40. Kovaleva VV, Kuznetsov NM, Istomina AP, et al. Low-filled suspensions of α-chitin nanorods for electrorheological applications. *Carbohydr Polym*. 2022;277:118792. doi:10.1016/j.carbpol.2021.118792
41. Geist MF, Boussois K, Smith A, Peyratout CS, Kurth DG. Nanocomposites derived from montmorillonite and metallosupramolecular polyelectrolytes: modular compounds for electrorheological fluids. *Langmuir*. 2013;29(6):1743-1747. doi:10.1021/la304657p
42. Schwarz G, Maisch S, Ullrich S, Wagenhöfer J, Kurth DG. Electrorheological fluids based on metallo-supramolecular polyelectrolyte-silicate composites. *ACS Appl Mater Interfaces*. 2013;5(10):4031-4034. doi:10.1021/am401104d
43. Kuznetsov NM, Zagoskin YD, Vdovichenko AY, et al. Enhanced electrorheological activity of porous chitosan particles. *Carbohydr Polym*. 2021;256:117530. doi:10.1016/j.carbpol.2020.117530
44. Han WJ, Lee JH, Choi HJ. Poly(diphenylamine)/polyaniline core/shell composite nanospheres synthesized using a reactive surfactant and their electrorheology. *Polymer*. 2020;188:122161. doi:10.1016/j.polymer.2020.122161
45. Plachý T, Žitka J, Mrlík M, et al. Electrorheology of polyindole. *Polymer*. 2021;217:123448. doi:10.1016/j.polymer.2021.123448
46. Chen Y, Sun W, Zheng H, et al. The electrorheological response behavior of small coral-like $H_2Ti_2O_5@SiO_2$ core-shell nanoparticles. *J Taiwan Inst Chem Eng*. 2021;129:327-341. doi:10.1016/j.jtice.2021.09.028
47. Kovaleva VV, Kuznetsov NM, Vdovichenko AY, Zagoskin YD, Grigoriev TE, Chvalun SN. Effect of temperature on the electrorheological behavior of porous chitosan particles in polydimethylsiloxane. *Dokl Phys Chem*. 2022;502:23-27. doi:10.1134/S0012501622020026
48. Park S, Gwon H, Lee S. Electroresponsive performances of ecoresorbable smart fluids consisting of various plant-derived carrier liquids. *Chemistry*. 2021;27(55):13739-13747. doi:10.1002/chem.202101597
49. Rejón L, Ramírez A, Paz F, Goycoolea FM, Valdez MA. Response time and electrorheology of semidiluted gellan, xanthan and cellulose suspensions. *Carbohydr Polym*. 2002;48(4):413-421. doi:10.1016/S0144-8617(01)00291-0
50. Yavuz M, Tilki T, Karabacak C, et al. Electrorheological behavior of biodegradable modified corn starch/corn oil suspensions. *Carbohydr Polym*. 2010;79(2):318-324. doi:10.1016/j.carbpol.2009.08.008
51. Kuznetsov NM, Zagoskin YD, Bakirov AV, et al. Is chitosan the promising candidate for filler in nature-friendly electrorheological fluids? *ACS Sustain Chem Eng*. 2021;9:3802-3810. doi:10.1021/acssuschemeng.0c08793
52. Sung JH, Choi HJ, Sohn JI, Jhon MS. Electrorheology of chitosan polysaccharide suspensions in soybean oil. *Colloid Polym Sci*. 2003;281(12):1196-1200. doi:10.1007/s00396-003-0909-y
53. Kuznetsov NM, Shevchenko VG, Stolyarova DY, Ozerin SA, Belousov SI, Chvalun SN. Dielectric properties of modified montmorillonites suspensions in polydimethylsiloxane. *J Appl Polym Sci*. 2018;135(46614):10. doi:10.1002/app.46614
54. Agafonov AV, Davydova OI, Krayev AS, et al. Unexpected effects of activator molecules' polarity on the electroreological activity of titanium dioxide nanopowders. *J Phys Chem B*. 2017;121(27):6732-6738. doi:10.1021/acs.jpcb.7b04131
55. Yoon CM, Lee S, Cheong OJ, Jang J. Enhanced electroresponse of alkaline earth metal-doped silica/titania spheres by synergetic effect of dispersion stability and dielectric property. *ACS Appl Mater Interfaces*. 2015;7(34):18977-18984. doi:10.1021/acsami.5b02388
56. Qiu Z, Shen R, Huang J, Lu K, Xiong X. A giant electrorheological fluid with a long lifetime and good thermal stability based on TiO_2 inlaid with nanocarbons. *J Mater Chem C*. 2019;7(19):5816-5820. doi:10.1039/c9tc00364a
57. Kuznetsov NM, Kovaleva VV, Zagoskin YD, et al. Specific features of the porous polymeric particle composites application as fillers for electrorheological fluids. *Nanobiotechnology Reports*. 2021;16(6):840-846. doi:10.1134/S2635167621060148
58. Grigoriev TE, Zagoskin YD, Belousov SI, et al. Influence of molecular characteristics of chitosan on properties of in situ formed scaffolds. *Bionanoscience*. 2017;7(3):492-495. doi:10.1007/s12668-017-0411-5
59. Vasilyev AV, Bukharova TB, Kuznetsova VS, et al. Comparison of impregnated bone morphogenetic protein-2 release kinetics from biopolymer scaffolds. *Inorg Mater Appl Res*. 2019;10(4):13-27. doi:10.1134/S2075113319050332
60. Rueden CT, Schindelin J, Hiner MC, et al. ImageJ2: ImageJ for the next generation of scientific image data. *BMC Bioinformatics*. 2017;18(1):1-26. doi:10.1186/s12859-017-1934-z
61. Franke D, Petoukhov MV, Konarev PV, et al. ATSAS 2.8: a comprehensive data analysis suite for small-angle scattering from macromolecular solutions. *J Appl Cryst*. 2017;50:1212-1225. doi:10.1107/S1600576717007786
62. Klimov DI, Zezina EA, Zubavichus YV, et al. Radiation induced generation of core-shell nanoparticles in polyelectrolyte films of poly(acrylic acid)-poly(ethylenimine) complex with copper and silver ions. *J Phys Chem C*. 2020;124(26):14409-14418. doi:10.1021/acs.jpcc.0c04882
63. Gonçalves C, Ferreira N, Lourenço L. Production of low molecular weight chitosan and chitooligosaccharides (COS): a review. *Polymers*. 2021;13(15):2466. doi:10.3390/polym13152466
64. Kiani H, Sun DW. Water crystallization and its importance to freezing of foods: a review. *Trends Food Sci Technol*. 2011;22(8):407-426. doi:10.1016/j.tifs.2011.04.011
65. Kasaai MR. A review of several reported procedures to determine the degree of N-acetylation for chitin and chitosan using infrared spectroscopy. *Carbohydr Polym*. 2008;71(4):497-508. doi:10.1016/j.carbpol.2007.07.009
66. Mirajkar S, Rathod P, Pawar B, Penna S, Dalvi S. γ-Irradiated chitosan mediates enhanced synthesis and antimicrobial properties of chitosan–silver (ag) nanocomposites. *ACS Omega*. 2021;6(50):34812-34822. doi:10.1021/acsomega.1c05358
67. Uznanski P, Zakrzewska J, Favier F, Kazmierski S, Bryszewska E. Synthesis and characterization of silver nanoparticles from (bis)alkylamine silver carboxylate precursors. *J Nanopart Res*. 2017;19(3):121. doi:10.1007/s11051-017-3827-5
68. Kumar-Krishnan S, Prokhorov E, Hernández-Iturriaga M, et al. Chitosan/silver nanocomposites: synergistic antibacterial action of silver nanoparticles and silver ions. *Eur Polym J*. 2015;67:242-251. doi:10.1016/j.eurpolymj.2015.03.066
69. Haq S, Rehman W, Waseem M, et al. Fabrication of pure and moxifloxacin functionalized silver oxide nanoparticles for photocatalytic and antimicrobial activity. *J Photochem Photobiol B Biol*. 2018;186:116-124. doi:10.1016/j.jphotobiol.2018.07.011
70. Shah A, Haq S, Rehman W, Waseem M, Shoukat S, ur-Rehman M. Photocatalytic and antibacterial activities of paeonia emodi mediated silver oxide nanoparticles. *Mater Res Express*. 2019;6(4):045045. doi:10.1088/2053-1591/aafd42
71. Marshall L, Zukoski CF IV, Goodwin JW. Effects of electric fields on the rheology of non-aqueous concentrated suspensions. *J Chem Soc, Faraday Trans 1*. 1989;85(9):2785-2795. doi:10.1039/f19898502785
72. Seo YP, Choi HJ, Seo Y. Analysis of the static yield stress for giant electrorheological fluids. *Korea Aust Rheol J*. 2017;29(3):215-218. doi:10.1007/s13367-017-0022-2
73. Vdovichenko AY, Kuznetsov NM, Shevchenko VG, Belousov SI, Yudina EB, Chvalun SN. The role of charge states in the self-organization of detonation nanodiamonds nanoparticles. *Diamond Relat Mater*. 2020;107(8):107903. doi:10.1016/j.diamond.2020.107903

74. Ivanov KV, Ivanova OS, Agafonov AV, Kozyukhin SA. The dielectric properties and flow of electrorheological fluids based on polymer-coated nanodispersed barium tetraacetate titanyl particles upon a dynamic shear in electric fields. *Colloid J*. 2017;79(2):204-211. doi:10.1134/S1061933X17020041
75. Liu YD, Choi HJ. Electrorheological fluids: smart soft matter and characteristics. *Soft Matter*. 2012;8(48):11961-11978. doi:10.1039/c2sm26179k
76. González-Campos JB, Prokhorov E, Luna-Bárcenas G, Fonseca-García A, Sanchez IC. Dielectric relaxations of chitosan: the effect of water on the α-relaxation and the glass transition temperature. *J Polym Sci B*. 2009;47(22):2259-2271. doi:10.1002/polb.21823

SUPPORTING INFORMATION

Additional supporting information can be found online in the Supporting Information section at the end of this article.

How to cite this article: Kuznetsov NM, Kovaleva VV, Volkov DA, et al. Porous chitosan particles doped by in situ formed silver nanoparticles: Electrorheological response in silicon oil. *Polym Adv Technol*. 2022;1-15. doi:10.1002/pat.5817